Current-induced magnetization reversal in NiFe/Cu/Co/Au notched mesoscopic bars

D. Morecroft,[1,2] I. A. Colin,[1] F. J. Castaño,[1] J. A. C. Bland,[2] and C. A. Ross[1]
[1]*Department of Materials Science and Engineering, Massachusetts Institute of Technology, Cambridge, Massachusetts 02139, USA*
[2]*Cavendish Laboratory, Cambridge University, Cambridge CB3 OHE, United Kingdom*
(Received 19 April 2007; published 29 August 2007)

In-plane current-induced and field-induced magnetization reversal in notched 2.1 μm long $\times$ 270 nm wide pseudo-spin-valve NiFe/Cu/Co/Au thin-film bars has been characterized and compared with the results of a three-dimensional micromagnetic model. The reversal of the soft NiFe layer is influenced by the magnetostatic fields of the hard Co layer, which can initiate switching of the NiFe layer from both ends of the bars, allowing for the existence of field-induced magnetic configurations containing one or two domain walls positioned at different notches. Current-induced reversal of both the NiFe and Co layers occurred for both directions of current flow in the presence of a bias field, and the reversal process differed from that found for field-induced reversal. Micromagnetic simulations including the Oersted field distribution created by the current pulses show that this term alone can account for the current-induced reversal.

DOI: 10.1103/PhysRevB.76.054449 PACS number(s): 75.47.−m, 85.75.Dd, 73.43.Qt, 85.70.Kh

I. INTRODUCTION

Current-induced magnetization switching (CIMS) has been proposed as an alternative to field-induced reversal for miniaturized (<150 nm) spintronic devices.[1,2] As the demand from industry for increased data storage density becomes greater, CIMS may provide a scalable write scheme for magnetic random access memory and other magnetoelectronic devices. Compared to conventional field-induced switching, CIMS offers the advantages of low power and simplified device architecture.

Much of the original work on CIMS was carried out by Berger and co-workers in the 1970s-1980s.[3–9] For thin ferromagnetic structures, the hydromagnetic drag force is negligible[3,10,11] and the interaction between the electric current and the magnetization is dominated by two effects: the Oersted field created by the current, and the spin-transfer torque due to *s-d* interaction between the spin-polarized electrons and the magnetic moments in the material. The spin-transfer effect can lead to the reversal of a single-domain magnetic structure or to the motion of a domain wall in a multidomain structure. Even in the absence of any external bias field, the effects of spin-transfer torque cannot always be easily distinguished from those of the Oersted field. The signature of the spin-transfer torque effect is that opposite current directions will lead to opposite domain wall motion. In contrast, the magnitude and local direction of the Oersted field from the pulsed current, and therefore, the wall motion, will depend on the magnetization state,[1] on layer sequence and geometry of the device (especially around the domain wall) as well as on the current direction.

Slonczewski[12] predicted that, for a multilayer thin-film structure such as a spin valve, in which each magnetic layer is a single domain,[13] current-induced spin-transfer torque can reverse the magnetization of one of the layers leading to a change in resistance. The current is polarized by one layer, and then exerts a torque on the second layer. CIMS with a current applied perpendicular to the plane of the layers (CPP) has been demonstrated with current densities of 10^{11}–10^{12} A/m^2 in several systems,[14–19] typically consisting of a hard and a soft magnetic layer of small lateral dimensions separated by a spacer layer. In such systems, the spin-transfer torque is expected to dominate over the effects of the Oersted field for devices below about 100 nm in diameter.[19]

Current-induced switching by domain wall motion has also been demonstrated extensively in thin ferromagnetic single-layer wires or bars. In these structures, the effect of the Oersted field is negligible[20] and the spin-polarized current exerts a torque on a domain wall, which translates the wall in the direction of the electron flux and/or leads to a change in the micromagnetic structure of the wall.[21–32] Threshold current densities are found to be of the same order of magnitude as those used to switch CPP multilayer devices. In single-layer thin-film devices, which are tested with the current applied in plane (CIP), the initial domain wall position has been controlled using nanoconstrictions,[21] zigzag lines,[22,23] and a pad and wire junction.[24,25] Wall motion in a variety of different shapes has also been investigated including U-shaped patterns[26,27] and ring structures.[28,29] Yamaguchi *et al.*[30] have measured a domain wall velocity that ranges from 2 to 6 m/s. The velocity is highly dependent on the micromagnetic structure of the wall.[22,23]

Compared to the cases of current-induced switching in CPP multilayer pillars and in CIP single-layer structures, there is relatively little work on current-induced switching in CIP multilayer structures. In the CIP geometry, the motion of a domain wall within a multilayer structure can be detected from the giant magnetoresistance (GMR), and this has been used to give a direct indication of the position of the wall.[31] Grollier *et al.*[31–34] investigated current-induced domain wall displacement in 20-μm-long CoO/Co/Cu/NiFe/Au spin-valve wires with widths down to 300 nm, where domain wall motion was obtained at current densities of the order of 10^{11}–10^{12} A/m^2. In narrow wires, both edge irregularities[32] and notches[31] were effective as domain wall pinning sites. The motion of a domain wall was found to be consistent with spin-transfer effects for zero or small bias fields ($H<7$ Oe), while at higher bias fields the current is believed to unpin the wall, which then moves under the influence of the applied field.

In this work, we have measured CIMS in 2.1-μm-long NiFe/Cu/Co/Au bars with widths of 270 nm, each contain-

 ©2007 The American Physical Society

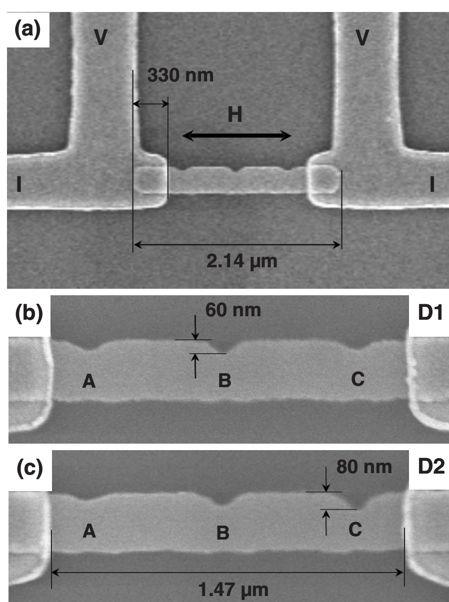

FIG. 1. Scanning electron micrographs of the devices. (a) The four-point electrical contact configuration and the applied field direction. (b) PSV bar with symmetric notch configuration, named D1. (c) PSV bar with an asymmetric notch configuration, named D2. The notches are labeled with letters A, B, and C.

ing three different notches with depths up to 80 nm. In these pseudo-spin-valve (PSV) bars, the magnetostatic coupling between the layers leads to reversal starting from both ends of the bars rather than by the movement of a single domain wall through the structure as occurs for longer bars. This, in turn, allows for one or two domain walls to be located within the bars, which can be moved using current pulses or applied fields. We will describe both field- and current-induced reversals, and show that the Oersted field from the current can lead to switching of the bars in the presence of a bias field.

II. EXPERIMENTAL METHODS AND MODELING

The bars were fabricated from a polycrystalline NiFe(6 nm)/Cu(4 nm)/Co(5 nm)/Au(4 nm) PSV stack grown onto a Si (100) wafer with 50-nm-thick thermal oxide. The fabrication procedure included a series of lithography and lift-off processing steps. The outer contact pads [Ti(5 nm)/Au(25 nm)] were defined using optical lithography, while both the notched PSV bars and the four contact wires [Ta(2 nm)/Cu(120 nm)] that connect the outer pads to the devices were defined in two separate aligned steps using electron-beam (e-beam) lithography. Figure 1(a) shows a scanning electron micrograph (SEM) of one of the PSV bars with four Ta/Cu electrical contacts. The devices investigated in the present work, named D1 and D2 in Figs. 1(b) and 1(c) for reference, consisted of 2.14-μm-long, 270-nm-wide PSV bars with rounded ends and three notches with different depths (labeled using letters A, B, and C). While the notch design in D1 is symmetric with respect to the center of the bar and contains notches with depths of 30, 60, and 30 nm, respectively, the notch configuration for D2 is asymmetric with respect to the center of the device and contains notches with depths of 30, 60, and 80 nm, respectively. Both devices were passivated using 80-nm-thick sputtered SiO_2.

The resistance of the bars was measured at room temperature with a four-point technique, using a constant rms current of 10 μA and ac lock-in detection at 1 kHz. The contact leads covered the ends of the bars [see Fig. 1(a)] and, since these leads are significantly thicker than the PSV stack, the changes in resistance measured for each bar are attributed to the 1.47-μm-long section of the bars located between the contact pads [see Figs. 1(b) and 1(c)]. The devices were placed on a precision goniometer rotary stage located between the poles of an electromagnet, which allowed for accurate alignment of the applied field along the axis of the bars. The field-induced magnetization reversal was explored by measuring resistance while sweeping the applied magnetic field. On the other hand, current-induced switching experiments were undertaken using current pulses of duration 10–100 μs, and amplitude ranging from 0.1 to 30 mA.

Micromagnetic simulations were carried out using the three-dimensional object oriented micromagnetic framework (OOMMF) simulation software.[35] The multilayer bars (D1 and D2) were discretized into $4\times4\times4$ nm^3 cubic cells with an in-plane shape that was determined by discretizing a micrograph of the device. Standard parameters were used for NiFe (exchange constant $A_{ex}=1.3\times10^{-6}$ erg/cm, saturation moment $M_s=860$ emu/cm^3, and magnetocrystalline anisotropy $K_1=5\times10^3$ erg/cm^3) and Co ($A_{ex}=3\times10^{-6}$ erg/cm, saturation moment $M_s=1400$ emu/cm^3, and $K_1=5.2\times10^6$ erg/cm^3), and the damping coefficient α was set to 0.5 to obtain rapid convergence. The magnetocrystalline anisotropy direction was set randomly in each cell to model a polycrystalline microstructure.

III. RESULTS AND DISCUSSION

A. Field-induced reversal

Figure 2(a) shows the resistance measured for both D1 and D2 on cycling the applied magnetic field. This behavior can be interpreted in terms of CIP giant magnetoresistance. The baseline resistance levels (159.2 and 192.0 Ω for D1 and D2, respectively) correspond to parallel alignment of the magnetizations of the Co and NiFe layers, while the highest levels (161.1 and 193.7 Ω for D1 and D2, respectively) correspond to the field ranges over which the NiFe and Co layers are magnetized antiparallel. The low-to-high resistance transitions, at which the NiFe reverses, occur at low applied fields (±50 Oe) through several intermediate resistance values. High-to-low resistance transitions, corresponding to the Co reversal, occur at moderate fields (±150–200 Oe). Clearly, while the transitions in the loop for D1 are symmetric with respect to zero field, the data for D2 are asymmetric, particularly for the moderate-field transitions.

The GMR ratio, defined as $[[\Delta R(H)\text{-}\Delta R(H_{max})]/\Delta R(H_{max})]\times100\%$, was 1.2% and 1.1% for D1 and D2, respectively. These rather low GMR ratios are similar to that of the unpatterned PSV film (1%) and result from current shunting by the Au and Cu layers. While the Cu spacer layer in these PSV bars is thick enough to consider exchange coupling between the NiFe and Co

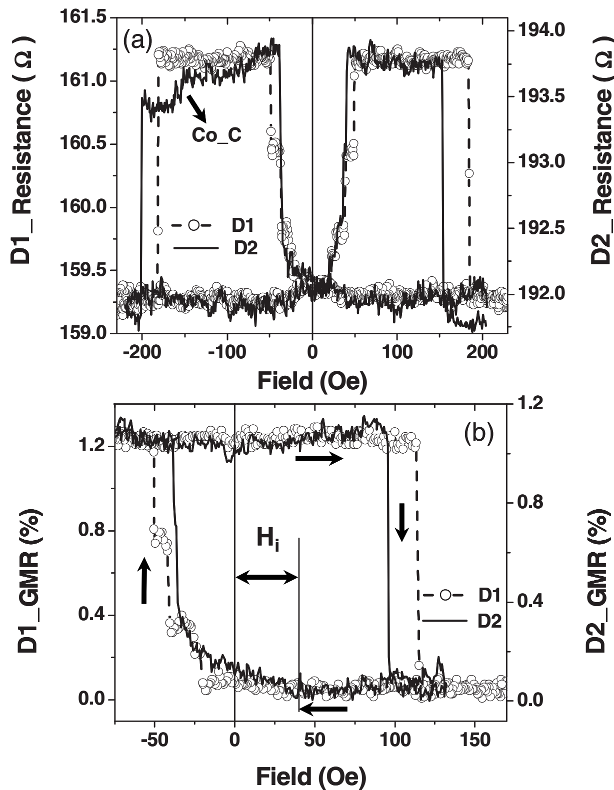

FIG. 2. (a) Magnetoresistance loops corresponding to the PSV bars with symmetric (D1) and asymmetric (D2) notch configurations with respect to the center of the bar. (b) Low-field GMR minor loops obtained on cycling the soft (NiFe) layer after saturating both D1 and D2 with a +1000 Oe field. The arrows indicate the cycling direction in the measurements and the shift of the center of the D1 loop with respect to zero applied field.

layers negligible,[36] this 4-nm-thick layer is sufficiently thin to allow for the NiFe and Co layers to be magnetostatically coupled, as found elsewhere in both unpatterned spin-valve films, as a result of the stray fields of domain walls,[37] and in patterned structures as a result of the stray fields from the edges of the layers.[38]

We now consider the low-field regime within which the NiFe layer reverses. Figure 3 shows dense low-field magnetoresistance loops measured at increments of 0.7 Oe of applied field, corresponding to the reversal of the NiFe soft layers in both PSV bars. By comparing the dimensions of the different sections of the bars defined by the positions of the notches with the magnitude of the switching fields and the relative height of these steps, a detailed picture of the NiFe reversal in both PSV bars may be deduced (see schematics in Fig. 3). This analysis unambiguously indicates that the soft layer reversal occurs from both ends of the bars, so that some of the stable intermediate resistance levels correspond to states in which two domain walls are present at different notches of the structures.

For D1, starting from the saturated state where the NiFe and Co layers are magnetized parallel, the first irreversible process at ∼−25 Oe involves the movement of a domain wall to notch A or C, reversing a small section of the bar at one side (described as state A or state C). At slightly larger fields, a second wall forms at notch C or A, reversing part of the bar at the other side (state AC). At −40 Oe, one of these two walls moves into the center notch, giving state AB or BC, and finally, the NiFe layer reverses completely at −50 Oe to give the antiparallel state. The reversal sequence is symmetric for both field directions. The intermediate states are stable at remanence, though this is not shown in the figure for clarity. For D2, a less symmetric reversal is found: for negative fields (right-to-left), there is little stability of intermediate states containing domain walls, though states C and BC can be discerned, while for positive fields, AC and BC can be identified. We attribute the small plateau at ∼±40 Oe to state BC rather than AB because it is most likely that the wall in notch A will move before the wall in notch C moves.

Reversal of the Co layer shows few intermediate states. D1 has no stable intermediate states, with abrupt reversal from the antiparallel to the parallel configuration at ∼180 Oe. D2 shows a similar abrupt reversal at 150 Oe for positive fields, but for negative fields the Co reverses from the right hand side only up to notch C (the deepest notch) at −150 Oe. Complete reversal only occurs at −200 Oe.

Minor loop cycling of the NiFe layer is shown in Fig. 2(b). After saturating the samples in either positive (as shown in the figure) or negative fields (not shown), cycling in fields up to ±180 Oe yields minor GMR loops that are asymmetric with respect to zero field and shifted along the positive or negative directions, respectively. The transition from the low resistance to high resistance states occurs below −50 Oe via several intermediate states, the same as those described above (Fig. 3). However, the high-to-low resistance transition occurs abruptly at significantly higher fields (114 and 95 Oe for D1 and D2, respectively). These switching fields are higher because the NiFe layer reversal is opposed by magnetostatic coupling from the Co layer. The shifts, H_i, in these minor loops with respect to zero field (38 and 30 Oe for D1 and D2, respectively) represent the strength of the coupling. These values are comparable or greater than the fields at which the intermediate states C, AC, BC, etc., form, which emphasizes the importance of magnetostatic coupling in the magnetization reversal of these structures. In comparison, magnetostatic effects are less important in the longer spin-valve bars previously used for CIMS studies, which show symmetric minor GMR loops[32] and reversal that occurs by the motion of a single domain wall along the structure.

Micromagnetic modeling of the field-induced switching of D1 and D2 depicts a reversal originating from both ends of the bars that is dominated by magnetostatic coupling. Due to the small thicknesses and width of the magnetic layers, the domain walls are head-to-head or tail-to-tail 180° transverse walls. Furthermore, the modeling shows that at remanence and at low applied fields (<100 Oe), significant tilting of the magnetization away from the long axis occurs for both magnetic layers (Fig. 4), in the vicinity of the notches and at the ends of the bars. At remanence and low applied fields, either “C-type” or “S-type” magnetization states can appear in each layer depending on the direction of the saturating field. The soft layer reversal initiates as the magnetization at the ends twists in an applied field, leading to two transverse domain walls with the same or opposite polarities. The magnetic con-

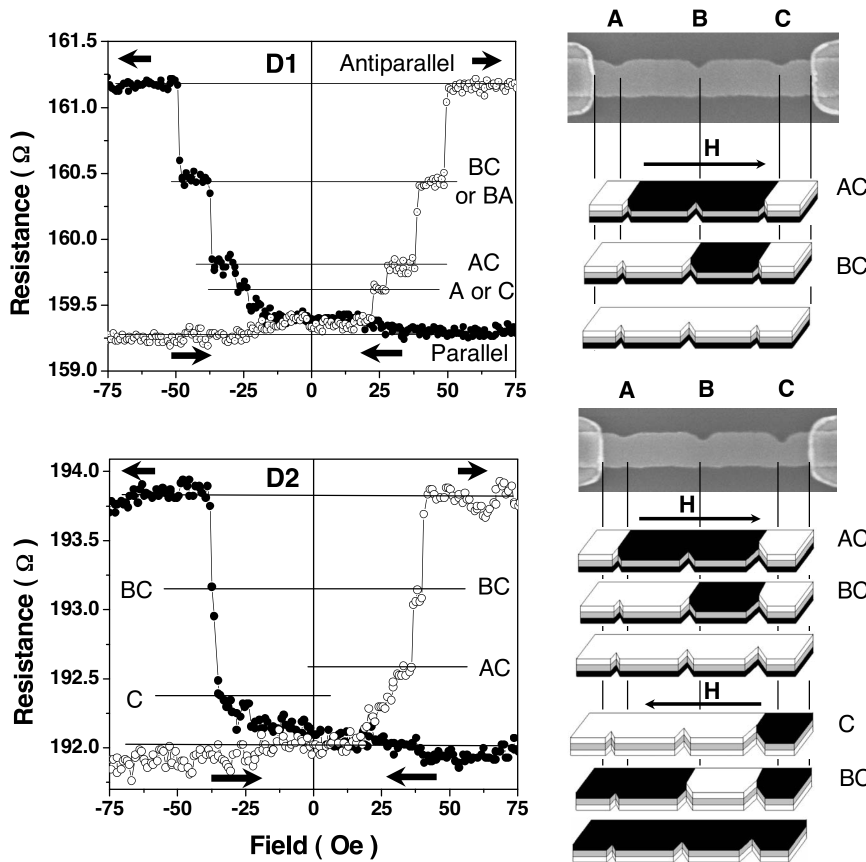

FIG. 3. Low-field magnetoresistance loops of the symmetric (D1) and asymmetric (D2) PSV bars and the corresponding notches for each intermediate resistance level. (Right) Corresponding SEMs and schematic representations of the reversal of the soft NiFe layer depicting the domain configurations as this layer transitions from parallel (lowest resistance, NiFe/Co black/black or white/white) to antiparallel (high resistance, NiFe/Co white/black or black/white) alignment with respect to the magnetization of the hard Co layer.

figurations at the ends of the NiFe layer are opposite in sense to those in the Co layer and are sensitive to the field cycling procedure used.

Overall, the results of field-induced reversal deduced from both magnetoresistance measurements and micromagnetic simulations indicate that these notched PSV bars can support a range of nonuniform magnetic configurations containing up to two domain walls. The locations of the walls in the notches at remanence or at low bias fields can be controlled by field cycling.

B. Pulsed current measurements

Figure 5(a) shows the resistance of D1 as a function of the pulse current amplitude and direction (with right-to-left and left-to-right electron flows in the bars being positive and negative, respectively), measured at bias fields corresponding to an AC domain wall configuration (see Fig. 3). The sample was initially saturated at +1000 Oe (or −1000 Oe) and then a bias field of 29.6 Oe was applied in the opposite direction to the saturating field. For each data point, a single current pulse was supplied to the bar followed by a resistance measurement to determine whether any reversal had occurred. This two-step procedure (pulse and resistance measurement) was repeated with increasing pulse amplitude for both possible current pulse directions.

For a positive bias field and negative current or negative bias field and positive current, two critical currents are observed, labeled I_{C1} and I_{C2}. Based on the resistance values, these represent respectively the partial reversal of the NiFe layer to form the BC or AB configuration (i.e., the movement of one wall into the center notch B) and the complete reversal of the NiFe (i.e., the unpinning of one of the walls and its annihilation with the other). The critical current densities range from 2×10^{11} to 5×10^{11} $\mathrm{A/m^2}$, which are of the same order of magnitude as those previously reported to move a domain wall in the soft layer of a spin-valve wire.[31–34] On

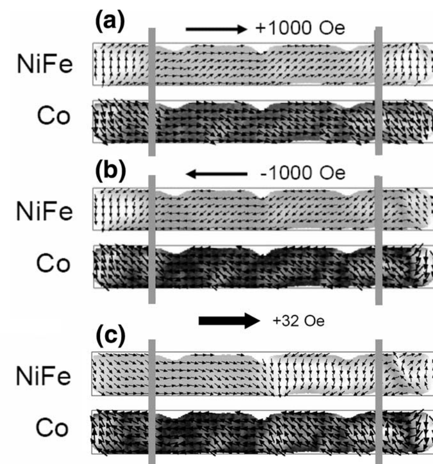

FIG. 4. [(a) and (b)] Micromagnetic simulations showing the remanent state in the NiFe and Co layers after applying +1000 and −1000 Oe saturating fields, respectively. (c) Micromagnetic snapshots corresponding to configurations in the NiFe and Co layers after saturating in a field of −1000 Oe and applying +32 Oe.

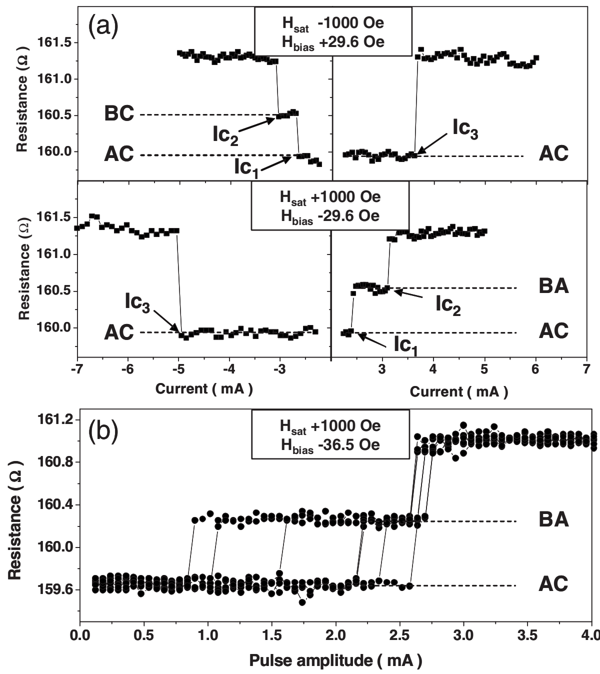

FIG. 5. (a) Resistance versus pulsed current measurements for D1 for both positive and negative field saturations, $\pm H_{\mathrm{sat}}$, and bias fields of ±29.6 Oe. I_{C1}, I_{C2}, and I_{C3} indicate the critical currents for domain wall movement. (b) Consecutive resistance versus pulse-amplitude measurements after positive saturation and application of −36.5 Oe bias.

the other hand, for a positive bias field and positive current, or negative bias field and negative current, the sample shows a single reversal step (I_{C3}) corresponding to the complete reversal of the NiFe. Even though CIMS occurred for both directions of the current flow, the response is asymmetric; for example, the two I_{C3} values in Fig. 5(a) are 3.5 and 5 mA. This asymmetry contrasts with the symmetric field-induced switching shown by D1.

Successive measurements on the same sample show a switching current distribution. As an example, Fig. 5(b) shows ten consecutive measurements for a bias of −36.5 Oe (starting from the AC state). The current I_{C1} required to propagate one of the walls from notch A or C to notch B varied between 0.8 and 2.6 mA, while the current I_{C2} required to unpin one of the domain walls to complete the reversal is quite consistent between measurements, varying only between 2.6 and 2.7 mA. A CIMS phase diagram for D1 is shown in Fig. 6, for a range of bias fields between 10 and 30 Oe. Error bars indicate the reproducibility of each critical current. This figure shows that as the bias field increases, the critical current required for reversal decreases. In both samples, CIMS could only be obtained in the presence of a bias field.

In contrast, CIMS experiments in D2 show a two-step switching response for all current and bias-field quadrants. Figure 7(a) shows the reversal at a bias field of ±37.5 Oe, which corresponds to a C or AC domain configuration. Reversing the soft layer from state C or AC into BC required current densities around 1.2×10^{11} A m^{-2}, while complete reversal from a BC configuration to the antiparallel state required higher current densities (up to 2×10^{12} A/m^2). Unlike D1, the variability in critical current was lower for I_{C1} than for I_{C2}. Figure 7(b) shows a series of ten consecutive CIMS measurements starting from state C, after saturating in +1000 Oe and applying a bias field of −35.2 Oe.

At higher bias fields, ~150 Oe, it was also possible to reverse the magnetization of the Co layers in a single step for both D1 and D2 using current densities around 1.2×10^{11} A/m^2 (not shown). For both devices, the maximum pulse current amplitude and maximum pulse length used were 30 mA and 100 μs, respectively. Higher values for

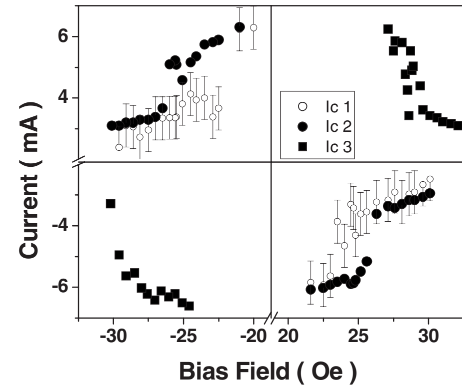

FIG. 6. CIMS phase diagram showing pulsed current amplitude versus bias field for D1. Open circles, full circles, and full squares correspond to critical switching currents I_{C1}, I_{C2}, and I_{C3}, respectively. For I_{C2} and I_{C3}, the error is within the size of the symbols.

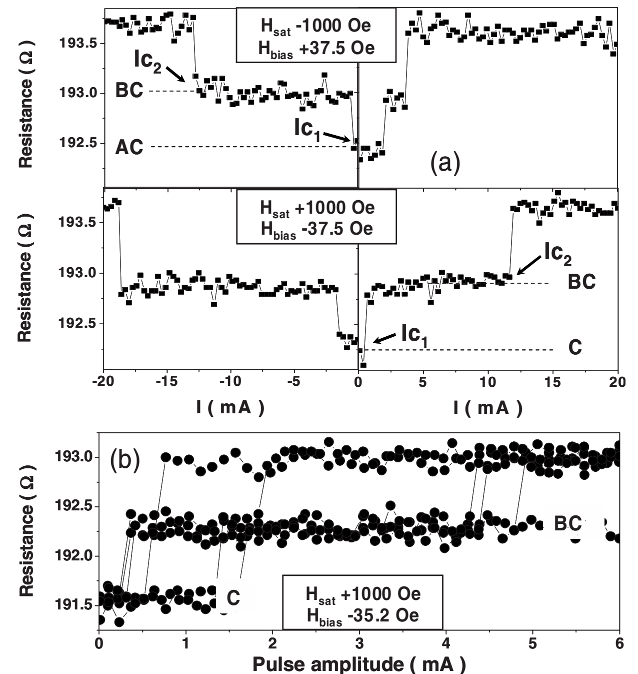

FIG. 7. (a) Resistance versus pulsed current amplitude measurements for D2 for both positive and negative field saturations, $\pm H_{\mathrm{sat}}$, and field bias of ±37.5 Oe (AC or A configurations). I_{C1} and I_{C2} indicate the critical currents for domain wall movement in the NiFe layer. (b) Consecutive resistance versus pulsed current measurements show the reproducibility of the critical currents I_{C1} and I_{C2} for a bias field of −35.2 Oe.

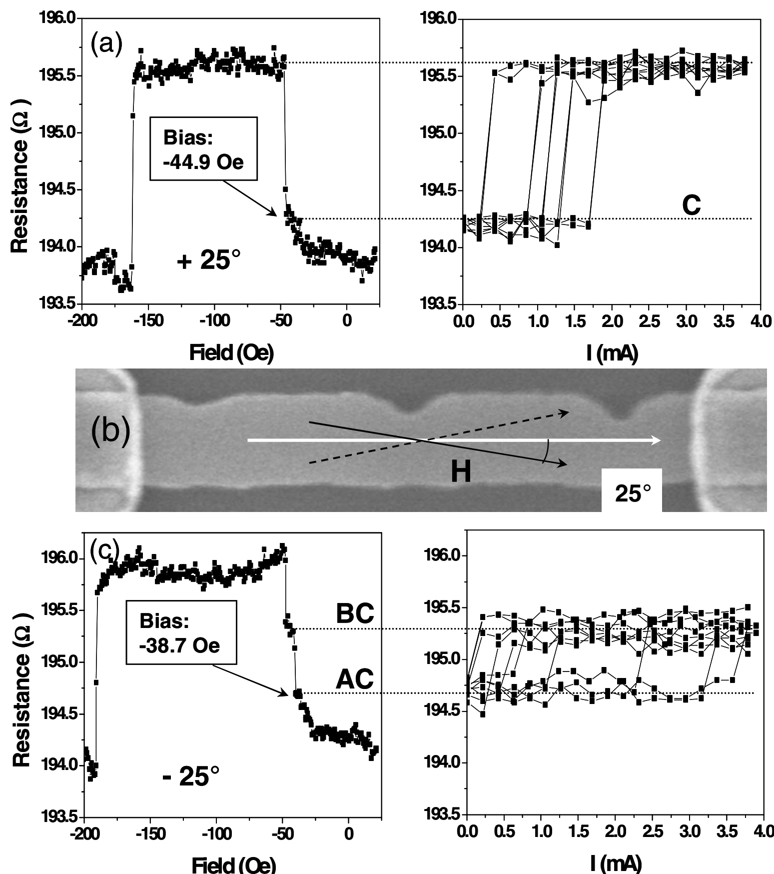

FIG. 8. (a) GMR measurements for D2 with the applied field at +25° (top left) and CIMS measurements in that configuration (top right) with an applied bias of −44.9 Oe. (b) Scanning electron microscopy image of D2 with the field and current highlighted to define the angle used. (c) GMR measurement at −25° with an applied bias of −38.7 Oe.

these parameters were not explored because they resulted in a slight increase in the resistance of the PSV bars, even though the switching fields for each transition in the GMR data remained unchanged.

Figure 8 shows how the angle between the axis of the bar and the external applied field can affect both the field-induced GMR data and the variability of the CIMS response. In this experiment, the saturation and bias fields are applied at +25° [Fig. 8(a)] or −25° [Fig. 8(b)] from the axis of D2. At +25°, the GMR indicates a single-step reversal with a variation in the critical current from 0.2 to 1.7 mA (a range of 1.5 mA) for a bias field of −44.9 Oe (corresponding to a domain wall at notch C). However, at −25°, the GMR data show that the soft layer at a bias of −38.7 Oe contains an AC configuration which only reverses to a BC configuration within the same current-amplitude range. These results suggest that the response of the soft layer to the transverse component of the field plays an important role in the reversal process.

The CIMS results show that the soft layer in each PSV bar can be reversed for all combinations of pulse current and bias-field direction to form the high resistance, antiparallel state. However, the lowest bias field for which CIMS was observed after saturation was 5 Oe for both devices. CIMS could not be observed at remanence for any of the possible domain wall configurations in either device for currents up to 30 mA. This contrasts with the results on longer bars with a single notch,[33] where current-induced reversal could be obtained at zero bias. In our experiment, the notches provide relatively strong pinning sites, and the current acting alone is insufficient to unpin the walls. The observations are consistent with reversal dominated by the bias field, in which the current pulse lowers the effective switching field.

C. Modeling

In order to investigate the importance of the Oersted field in the current-induced reversal of these structures, micromagnetic simulations were carried out, in which the Oersted field term was included. The Oersted field distribution in the NiFe layer was calculated based on the resistivities of the four layers. The resistivity of each metallic layer was measured from single-layer films of 6 nm NiFe (87 $\mu\Omega$ cm), 4 nm Cu (90 $\mu\Omega$ cm), 5 nm Co (30.5 $\mu\Omega$ cm), and 4 nm Au (49 $\mu\Omega$ cm), sputter deposited onto Si (100) wafers with 50-nm-thick thermal oxide. A parallel resistor model predicts a net resistance of the PSV structure of 6Ω, while the measured resistance was 3.7 Ω, indicating that the mean free path of the electrons exceeds the layer thicknesses. The parallel resistor model predicts a current distribution within each layer of 19.25% in NiFe, 12.32% in Cu, 45.62% in Co, and 22.81% in Au. (A longer mean free path will make the current distribution more homogeneous.) Each layer in the bar was then modeled as an array of 1.4-μm-long finite wires placed every 1 nm in the y and z directions. as depicted in Fig. 9. The Biot-Savart law[39] was used to derive the Oersted field distribution in the NiFe layer from the current. The results of the calculation for a cross section at the center of

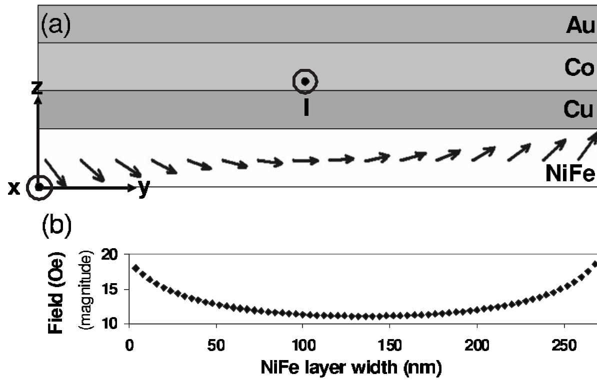

FIG. 9. (a) Oersted field distribution in a section at the center of the bar for a positive current density of 5×10^{11} A/m^2. The magnitude of the Oersted field along the width of the bar is shown in (b).

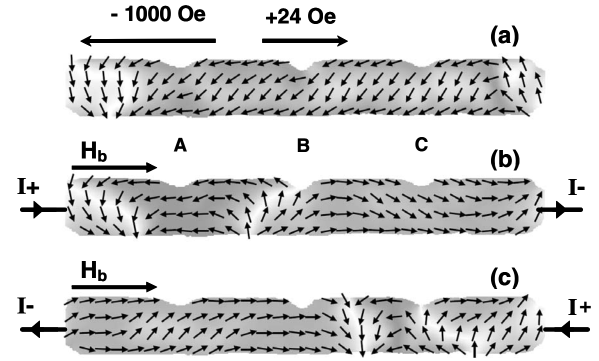

FIG. 10. Simulation results showing the effect of the Oersted field from the pulsed current on the magnetization state in the soft magnetic layer. (a) The remanent magnetization state after applying a negative saturation field (H_s) and a small positive bias field (H_b). [(b) and (c)] Minimized energy states after pulsing a current in the positive and negative directions in the presence of a bias field.

the bar are shown in Fig. 9 for a current density of 5×10^{11} A/m^2. The field has a nontrivial in-plane component in the y direction, perpendicular to the bar, and its magnitude varies between 10 and 20 Oe [Fig. 9(b)]. This model neglects the effect of the notches, but it is expected that notches will also produce a local component of the Oersted field along the x direction. The Oersted field in the hard layer was not taken into account since its magnitude added to the bias field remains much smaller than the switching values found in the GMR data.

The calculated Oersted field distribution was included in the micromagnetic simulations of sample D1. Figure 10(a) shows the magnetization state in the NiFe layer after applying a negative saturation field of −1000 Oe followed by a small positive bias field of +24 Oe. For D1, experimentally this bias corresponds to a domain wall at notch A or C, in agreement with the small plateau evident at this field in Fig. 3. In the model, we see partial reversal near the left end of the bar. Figures 10(b) and 10(c) show the magnetization state after applying a positive and negative current pulse of density 5×10^{11} A/m^2 for 5 ns (Ref. 40), respectively, and then minimizing the energy in the presence of the bias field for positive and negative current directions, respectively. The results show an asymmetric reversal in the soft layer with respect to the direction of the current pulse. Notably, the reversal in each case starts from opposite ends of the bar, and different volumes of the bar have reversed for each current direction. For positive current, domain walls remain near notches A and B, while for the negative current direction, the NiFe layer is almost completely reversed, with one wall past notch B and another near notch C. For both current directions, the NiFe is partly reversed and the resistance would increase, but the details of the reversal differ. These characteristics agree qualitatively with the experimental observations. The simulations indicate that the Oersted field term alone is capable of promoting reversal in the soft magnetic layer in a bias field to achieve a change in GMR, even in the absence of a spin torque effect.

IV. SUMMARY

The field- and current-induced reversal of 2.1-μm-long, 270-nm-wide Co/Cu/NiFe notched bars have been investigated using measurements of giant magnetoresistance combined with three-dimensional micromagnetic modeling. In the major hysteresis loops, the soft NiFe layer reversal is initiated from the ends of the bar under the influence of the magnetostatic field from Co. Several intermediate resistance states may be identified corresponding to the presence of domain walls located at the notches. Domain wall movement can be accomplished in both the soft and hard layers of the PSV using current densities of order 10^{11} A/m^2, in the presence of a biasing magnetic field. The critical current for domain wall movement decreases as the bias field is increased, but in these samples, current-induced reversal was not obtained in bias fields below 5 Oe. Reversal of the NiFe layer occurs in either a single-step or a two-step process depending on the notch configuration and the direction of bias field and current. Current-induced magnetization reversal of the Co layer occurs as a single step for both current and bias-field directions.

These small structures show significant magnetostatic interactions between the NiFe and Co layers and effective pinning of domain walls at the notches. The reversal of the NiFe is driven primarily by the bias field, while the Oersted field from the current pulse promotes reversal at bias fields below the switching field. In these small current-in-plane multilayer structures, modeling indicates that the Oersted field from the current pulse is sufficient to promote domain wall depinning in the soft layer, even in the absence of spin torque effects.

ACKNOWLEDGMENTS

The authors would like to thank H. I. Smith for the use of nanofabrication facilities. This work was supported by the Marie Curie Foundation, the National Science Foundation, the NERC INDEX Program, and the Singapore-MIT alliance.

[1] C. H. Marrows, Adv. Phys. **54**, pg 585 (2005).
[2] S. S. P. Parkin, U.S. Patent No. 6,834,005 (2004).
[3] L. Berger, J. Phys. Chem. Solids **35**, 947 (1974).
[4] L. Berger, J. Appl. Phys. **49**, 2156 (1978).
[5] L. Berger, J. Appl. Phys. **55**, 1954 (1984).
[6] P. P. Freitas and L. Berger, J. Appl. Phys. **57**, 1266 (1985).
[7] C.-Y. Hung and L. Berger, J. Appl. Phys. **63**, 4276 (1988).
[8] L. Berger, J. Appl. Phys. **71**, 2721 (1992).
[9] E. Salhi and L. Berger, J. Appl. Phys. **76**, 4787 (1994).
[10] W. J. Carr, J. Appl. Phys. **45**, 394 (1974).
[11] S. H. Charap, J. Appl. Phys. **45**, 397 (1974).
[12] J. C. Slonczewski, J. Magn. Magn. Mater. **159**, L1 (1996).
[13] M. Tsoi, A. G. M. Jansen, J. Bass, W.-C. Chiang, M. Seck, V. Tsoi, and P. Wyder, Phys. Rev. Lett. **80**, 4281 (1998).
[14] E. B. Myers, D. C. Ralph, J. A. Katine, R. N. Louie, and R. A. Buhrman, Science **285**, 867 (1999).
[15] S. J. C. H. Theeuwen, J. Caro, K. P. Wellock, S. Radelaar, C. H. Marrows, B. J. Hickey, and V. I. Kozub, Appl. Phys. Lett. **75**, 3677 (1999).
[16] J. A. Katine, F. J. Albert, R. A. Buhrman, E. B. Myers, and D. C. Ralph, Phys. Rev. Lett. **84**, 3149 (2000).
[17] J. Grollier, V. Cros, A. Hamzić, J. M. George, H. Jaffrès, A. Fert, G. Faini, J. Ben Youssef, and H. Legall, Appl. Phys. Lett. **78**, 3663 (2001).
[18] H. Yi, T. H. Y. Nguyen, J. Chang, and K. H. Shin, J. Vac. Sci. Technol. B **23**, 339 (2005).
[19] J. Z. Sun, IBM J. Res. Dev. **50**, 81 (2006).
[20] A. Thiaville, Y. Nakatani, J. Miltat, and Y. Suzuki, Europhys. Lett. **69**, 990 (2005).
[21] M. Tsoi, R. E. Fontana, and S. S. P. Parkin, Appl. Phys. Lett. **83**, 2617 (2003).
[22] M. Kläui, P.-O. Jubert, R. Allenspach, A. Bischof, J. A. C. Bland, G. Faini, U. Rüdiger, C. A. F. Vaz, L. Vila, and C. Vouille, Phys. Rev. Lett. **95**, 026601 (2005).
[23] M. Kläui, M. Laufenberg, L. Heyne, D. Backes, U. Rüdiger, C. A. F. Vaz, J. A. C. Bland, L. J. Heyderman, S. Cherifi, A. Locatelli, T. O. Mentes, and L. Aballe, Appl. Phys. Lett. **88**, 232507 (2006).
[24] K. Kimura, Y. Otani, K. Tsukagoshi, and Y. Aoyagi, J. Appl. Phys. **94**, 7947 (2003).
[25] K. Kimura, Y. Otani, I. Yagi, K. Tsukagoshi, and Y. Aoyagi, J. Appl. Phys. **94**, 7266 (2003).
[26] N. Vernier, D. A. Allwood, D. Atkinson, M. D. Cooke, and R. P. Cowburn, Europhys. Lett. **65**, 526 (2004).
[27] J. L. Tsai, S. F. Lee, Y. Liou, Y. D. Yao, T. Y. Chen, and K. W. Cheng, J. Appl. Phys. **97**, 10C710 (2005).
[28] M. Kläui, C. A. F. Vaz, J. A. C. Bland, W. Wernsdorfer, G. Faini, E. Cambril, and L. J. Heyderman, Appl. Phys. Lett. **83**, 105 (2003).
[29] M. Kläui, C. A. F. Vaz, J. A. C. Bland, W. Wernsdorfer, G. Faini, E. Cambril, L. J. Heyderman, F. Nolting, and U. Rüdiger, Phys. Rev. Lett. **94**, 106601 (2005).
[30] A Yamaguchi, T. Ono, S. Nasu, K. Miyake, K. Mibu, and T. Shinjo, Phys. Rev. Lett. **92**, 077205 (2004).
[31] J. Grollier, D. Lacour, V. Cros, A. Hamzić, A. Vaurès, A. Fert, D. Adam, and G. Faini, J. Appl. Phys. **92**, 4825 (2002).
[32] J. Grollier, P. Boulenc, V. Cros, A. Hamzić, A. Vaurès, A. Fert, and G. Faini, Appl. Phys. Lett. **83**, 509 (2003).
[33] J. Grollier, P. Boulenc, V. Cros, A. Hamzić, A. Vaurès, A. Fert, and G. Faini, J. Appl. Phys. **95**, 6777 (2004).
[34] C. K. Lim, T. Devolder, C. Chappert, J. Grollier, V. Cros, A. Vaurès, A. Fert, and G. Faini, Appl. Phys. Lett. **84**, 2820 (2004).
[35] http://math.nist.gov/oommf
[36] H. W. Fuller and D. L. Sullivan, J. Appl. Phys. **33**, 1063 (1962).
[37] H. D. Chopra, D. X. Yang, P. J. Chen, D. C. Parks, and W. F. Egelhoff, Phys. Rev. B **61**, 9642 (2000).
[38] F. J. Castaño, D. Morecroft, and C. A. Ross, Phys. Rev. B **74**, 224401 (2006).
[39] Z. Qihou, Eur. J. Phys. **8**, 128 (1987).
[40] K.-J. Lee and B. Dieny, Appl. Phys. Lett. **88**, 132506 (2006).